Searches for multi-Z boson productions and anomalous gauge boson couplings at a muon collider*

Ruobing Jiang (蒋若冰) Chuqiao Jiang (蒋楚翘)† Alim Ruzi Tianyi Yang (杨天一)
Yong Ban (班勇) Qiang Li (李强)

School of Physics and State Key Laboratory of Nuclear Physics and Technology, Peking University, Beijing 100871, China

Abstract: Multi-boson productions can be exploited as novel probes either for standard model precision tests or new physics searches, and have become a popular research topic in ongoing LHC experiments and future collider studies, including those for electron–positron and muon–muon colliders. In this study, we focus on two examples, *i.e.*, ZZZ direct productions through $\mu^+\mu^-$ annihilation at a 1 TeV muon collider, and ZZ productions through vector boson scattering (VBS) at a 10 TeV muon collider, with an integrated luminosity of 10 ab^{-1}. Various channels are considered, including ZZZ $\to 4\ell 2\nu$ and ZZZ $\to 4\ell$+2jets. The expected significance on these multi-Z boson production processes is reported based on a detailed Monte Carlo study and signal background analysis. Sensitivities on anomalous gauge boson couplings are also presented.

Keywords: TeV physics, muon collider, multi-Z boson, anomalous quartic gauge boson interactions

DOI: 10.1088/1674-1137/ad5661

I. INTRODUCTION

The Standard Model (SM) is based on the $SU(3)_C\otimes SU(2)_L\otimes U(1)_Y$ gauge symmetry group and describes the interactions among all elementary particles [1]. The discovery of the Higgs boson by the CMS and ATLAS experiments [2, 3] at the Large Hadron Collider (LHC) in 2012 marks a great success of SM physics. The high-luminosity LHC (HL-LHC), together with other future colliders, such as muon colliders, will not only enable researchers to make more precise measurements on characteristic properties of SM physics but also to unravel undiscovered phenomena beyond SM physics.

Recently, a muon collider working at a centre of mass (COM) energy at the TeV scale has received revived interest from the community of high-energy physics [4, 5]. Given that muons are approximately 200 times heavier than electrons, the energy loss caused by synchrotron radiation for muons is much less than that for electrons. Moreover, muon-muon collisions provide a cleaner environment than proton-proton collisions. These features make muon colliders attractive energy-efficient machines to explore high-energy physics.

A muon collider offers numerous opportunities to study elementary particle physics [6, 7]. For instance, when the COM energy is around 1 TeV, $\mu^+\mu^-$ annihilation acts as the dominant production mechanism. At the multi-TeV scale, muons have a high probability to emit electroweak (EW) radiation. Therefore, a high-energy muon collider can also serve as a vector boson collider. Both collision modes provide a spectacular playground for both the search for the origin of EW symmetry breaking (EWSB) and for EW interactions beyond the Standard Model, such as anomalous gauge boson interactions [8−14].

For current and future colliders, multi-boson production is an interesting topic, sensitive to the non-abelian character of the SM [1, 15]. In particular, the presence of anomalous quartic gauge boson interactions [16−18] can be probed through tri-boson production and through di-boson production via vector boson scattering. Many studies have been published on this topic at the LHC [19, 20]. In this study, we focussed on two examples, *i.e.*, ZZZ direct productions through $\mu^+\mu^-$ annihilation at a 1 TeV muon collider, and ZZ productions through the VBS process at a 10 TeV muon collider, with an integrated luminosity of 10 ab^{-1}.

Received 3 April 2024; Accepted 6 June 2024; Published online 7 June 2024

* Supported in part by the National Natural Science Foundation of China (12150005, 12075004, 12061141002) and MOST (2018YFA0403900)

† E-mail: chuqiao.jiang@cern.ch

II. MULTI-BOSON AND ANOMALOUS QUARTIC GAUGE COUPLINGS

Precision measurements of multi-boson production allow a basic test of the SM and provide a model-independent method to search for BSM at the TeV scale [19]. In this study, we focussed on ZZZ direct productions and ZZ productions through vector boson scattering. Both processes are sensitive to non-abelian gauge boson interactions and the structure of EW symmetry breaking. These multi-boson processes represent an important avenue to test anomalous triple gauge couplings (aTGCs) and anomalous quartic gauge couplings (aQGCs) [1], as well as to search for possible modifications of these vertices from new physics [20].

Anomalous modifications of gauge couplings can be parameterized through the effective field theory (EFT) by adding higher order modifications to the SM Lagrangian:

$$\mathcal{L}^{NP} = \mathcal{L}^{4(SM)} + \frac{1}{\Lambda}\mathcal{L}^{5} + \frac{1}{\Lambda^2}\mathcal{L}^{6} + \frac{1}{\Lambda^3}\mathcal{L}^{7} + \frac{1}{\Lambda^4}\mathcal{L}^{8} + ... \quad (1)$$

The higher order terms are suppressed by mass scale Λ, which represents the scale of new physics beyond the SM. The terms featuring odd dimensions are not considered because they will not influence multi-boson production measurements. The dimension-6 operators are related to aTGCs, whereas the dimension-8 operators are related to aQGCs.

Note that aQGCs can be realized by introducing new heavy bosons, which contribute to aQGCs at the tree level, while one loop is suppressed in aTGCs [16, 21, 22]. Furthermore, given that numerous experimental tests of aTGCs have shown good agreement with the SM, this study mainly focused on genuine aQGCs.

To express the aQGC contributions in a model-independent manner, an EFT of the EW breaking sector [16, 23−27] is utilized. When $SU(2)_L \otimes U(1)_Y$ is represented linearly, the lowest order genuine aQGC operators parameterized in the EFT are dimension-8 (dim-8) [25, 27−29]. The genuine aQGC operators can be expressed as follows [30]:

$$\begin{aligned}
O_{S,0} &= \left[\left(D_\mu\Phi\right)^\dagger D_\nu\Phi\right] \times \left[\left(D^\mu\Phi\right)^\dagger D^\nu\Phi\right], \\
O_{S,1} &= \left[\left(D_\mu\Phi\right)^\dagger D^\mu\Phi\right] \times \left[\left(D_\nu\Phi\right)^\dagger D^\nu\Phi\right], \\
O_{S,2} &= \left[\left(D_\mu\Phi\right)^\dagger D_\nu\Phi\right] \times \left[\left(D^\nu\Phi\right)^\dagger D^\mu\Phi\right], \\
O_{M,0} &= \mathrm{Tr}\left[\widehat{W}_{\mu\nu}\widehat{W}^{\mu\nu}\right] \times \left[\left(D_\beta\Phi\right)^\dagger D^\beta\Phi\right], \\
O_{M,1} &= \mathrm{Tr}\left[\widehat{W}_{\mu\nu}\widehat{W}^{\nu\beta}\right] \times \left[\left(D_\beta\Phi\right)^\dagger D^\mu\Phi\right], \\
O_{M,2} &= \left[B_{\mu\nu}B^{\mu\nu}\right] \times \left[\left(D_\beta\Phi\right)^\dagger D^\beta\Phi\right] \\
O_{M,3} &= \left[B_{\mu\nu}B^{\nu\beta}\right] \times \left[\left(D_\beta\Phi\right)^\dagger D^\mu\Phi\right], \\
O_{M,4} &= \left[\left(D_\mu\Phi\right)^\dagger \widehat{W}_{\beta\nu} D^\mu\Phi\right] \times B^{\beta\nu}, \\
O_{M,5} &= \left[\left(D_\mu\Phi\right)^\dagger \widehat{W}_{\beta\nu} D^\nu\Phi\right] \times B^{\beta\mu} + \mathrm{h.c.}, \\
O_{M,7} &= \left[\left(D_\mu\Phi\right)^\dagger \widehat{W}_{\beta\nu}\widehat{W}^{\beta\mu} D^\nu\Phi\right], \\
O_{T,0} &= \mathrm{Tr}\left[\widehat{W}_{\mu\nu}\widehat{W}^{\mu\nu}\right] \times \mathrm{Tr}\left[\widehat{W}_{\alpha\beta}\widehat{W}^{\alpha\beta}\right], \\
O_{T,1} &= \mathrm{Tr}\left[\widehat{W}_{\alpha\nu}\widehat{W}^{\mu\beta}\right] \times \mathrm{Tr}\left[\widehat{W}_{\mu\beta}\widehat{W}^{\alpha\nu}\right], \\
O_{T,2} &= \mathrm{Tr}\left[\widehat{W}_{\alpha\mu}\widehat{W}^{\mu\beta}\right] \times \mathrm{Tr}\left[\widehat{W}_{\beta\nu}\widehat{W}^{\nu\alpha}\right], \\
O_{T,3} &= \mathrm{Tr}\left[\widehat{W}_{\mu\nu}\widehat{W}_{\alpha\beta}\right] \times \mathrm{Tr}\left[\widehat{W}^{\alpha\nu}\widehat{W}^{\mu\beta}\right], \\
O_{T,4} &= \mathrm{Tr}\left[\widehat{W}_{\mu\nu}\widehat{W}_{\alpha\beta}\right] \times B^{\alpha\nu}B^{\mu\beta}, \\
O_{T,5} &= \mathrm{Tr}\left[\widehat{W}_{\mu\nu}\widehat{W}^{\mu\nu}\right] \times B_{\alpha\beta}B^{\alpha\beta}, \\
O_{T,6} &= \mathrm{Tr}\left[\widehat{W}_{\alpha\nu}\widehat{W}^{\mu\beta}\right] \times B_{\mu\beta}B^{\alpha\nu}, \\
O_{T,7} &= \mathrm{Tr}\left[\widehat{W}_{\alpha\mu}\widehat{W}^{\mu\beta}\right] \times B_{\beta\nu}B^{\nu\alpha}, \\
O_{T,8} &= B_{\mu\nu}B^{\mu\nu}B_{\alpha\beta}B^{\alpha\beta}, \\
O_{T,9} &= B_{\alpha\mu}B^{\mu\beta}B_{\beta\nu}B^{\nu\alpha}.
\end{aligned} \quad (2)$$

Here, Φ denotes the Higgs doublet, the covariant derivative is given by $D_\mu\Phi = \left(\partial_\mu + \mathrm{i}gW_\mu^j\frac{\sigma^j}{2} + \mathrm{i}g'B_\mu\frac{1}{2}\right)\Phi$, σ^j ($j = 1,2,3$) represents the Pauli matrices, $\widehat{W}_{\mu\nu} \equiv W^j_{\mu\nu}\frac{\sigma^j}{2}$ is the $SU(2)_L$ field strength, and $B_{\mu\nu}$ denotes the $U(1)_Y$ one. The effective Lagrangian with the contributions from genuine aQGC operators can be expressed as follows:

$$\begin{aligned}
\mathcal{L}_{\mathrm{eff}} &= \mathcal{L}_{SM} + \mathcal{L}_{\mathrm{anomalous}} \\
&= \mathcal{L}_{SM} + \sum_{d>4}\sum_i \frac{f_i^{(d)}}{\Lambda^{d-4}}O_i^{(d)} \\
&= \mathcal{L}_{SM} + \sum_i \left[\frac{f_i^{(6)}}{\Lambda^2}O_i^{(6)}\right] + \sum_j \left[\frac{f_j^{(8)}}{\Lambda^4}O_i^{(8)}\right] + ...,
\end{aligned} \quad (3)$$

where Λ is the characteristic scale and $f_j^{(8)}/\Lambda^4 = f_{S,j}/\Lambda^4$, $f_{M,j}/\Lambda^4$, $f_{T,j}/\Lambda^4$ represents the coefficients of the corresponding aQGC operators [27]. These coefficients are expected to be zero in the SM prediction.

In this study, we are interested in multi-Z productions, which are rare processes yet to be observed. BSM may introduce measurable contributions and result in deviations from the SM prediction. Examples of processes related to ZZZ production in the SM and from the aQGC operator are depicted in Fig. 1, while those for VBS ZZ production are shown in Fig. 2.

III. SIMULATION AND ANALYSIS FRAMEWORK

Both the signal and background events were generated with MadGraph5_aMC@NLO [31, 32] at the parton level. Subsequently, they were showered and hadronized through PYTHIA 8.3 [33]. The effects of aQGC operators were simulated with MadGraph5_aMC@NLO using the Universal FeynRules Output module [34, 35]. The SM processes were simulated with the default SM model. DELPHES [36] version 3.0 was used to simulate detect-

or effects, with settings for a muon collider detector [37]. Jets were clustered from the reconstructed stable particles (except electrons and muons) using FASTJET [38], with the k_T algorithm having a fixed cone size of $R_{\rm jet} = 0.5$.

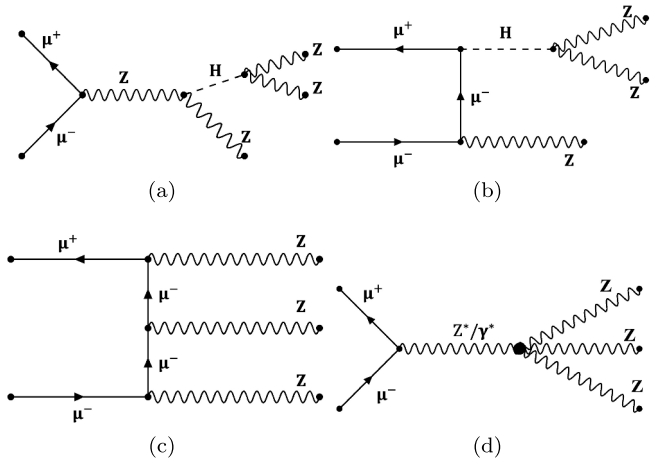

Fig. 1. Examples of Feynman diagrams of ZZZ production processes at a muon collider: (a-c) are from the SM and (d) involves quartic gauge couplings.

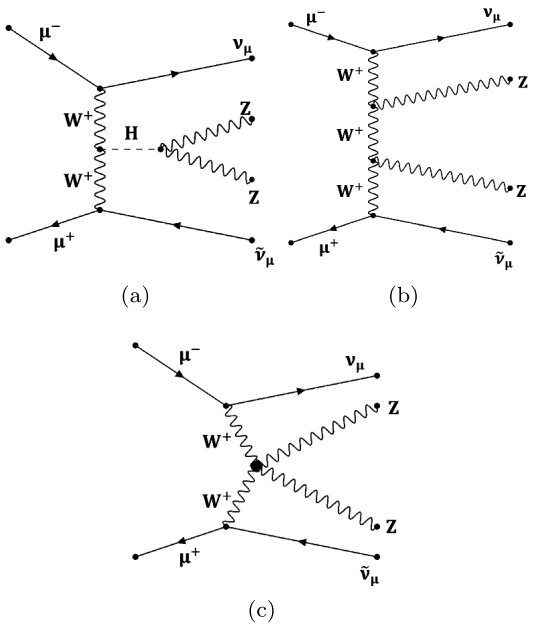

Fig. 2. Examples of Feynman diagrams of VBS ZZ production processes at a muon collider: (a) and (b) are from the SM and (c) involves quartic gauge couplings.

Two collider scenarios and benchmarks for multi-Z productions were considered: 1) a COM energy of $\sqrt{s} = 1$ TeV for ZZZ direct productions, and 2) a 10 TeV scale muon collider, where VBS [39] is the dominant production should be replaced by "mechanism, of which the general VBS Feynman diagram is shown in Fig. 3, which includes our VBS ZZ signal process. Both scenarios were studied at an integral luminosity of $10\,{\rm ab}^{-1}$.

In the study of the tri-Z boson production at a muon collider, we focused on either a pure leptonic decay, $\mu^+\mu^- \to {\rm ZZZ} \to \ell_1^+\ell_1^-\ell_2^+\ell_2^-\nu_3\bar{\nu}_3$, or a semi-leptonic decay, $\mu^+\mu^- \to {\rm ZZZ} \to \ell_1^+\ell_1^-\ell_2^+\ell_2^- jj$, where ℓ denotes the electron or muon and j denotes the jet. In the study of the ZZ productions through VBS, we considered a pure-leptonic channel, $\mu^+\mu^- \to {\rm ZZ}\nu_\mu\bar{\nu}_\mu \to 4\ell + \nu_\mu\bar{\nu}_\mu$, and a semi-leptonic channel, $\mu^+\mu^- \to {\rm ZZ}\nu_\mu\bar{\nu}_\mu \to 2\ell 2j + \nu_\mu\bar{\nu}_\mu$. The interference effect was included in our simulations with MadGraph. Backgrounds were classified into several categories:

• P1: s-channel processes:
– $\mu^+\mu^- \to X = at\bar{t} + bV + c{\rm H}$, with a, b, c as integers.

• P2: VBS processes further divided into [40]:
– P2.1: $\rm W^+W^-$ fusion with two neutrinos in the final state, denoted as WW_VBS below.
– P2.2 $ZZ/Z\gamma/\gamma\gamma$ fusion with two muons in the final state, denoted as ZZ_VBS below.
– P2.3: $\rm W^\pm Z/W^\pm\gamma$ fusion with one muon and one neutrino in the final state, denoted as WZ_VBS below.

We list all considered backgrounds in Table 1.

Multi-Z signals studied herein have a very small cross section, whereas the backgrounds are extremely large. Therefore, it is necessary to apply selections to optimize

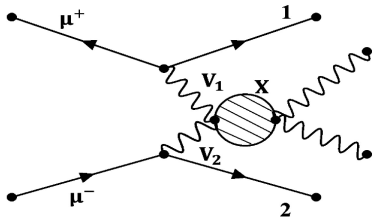

Fig. 3. Example of diagram of VBS processes at a muon collider.

Table 1. Summary of the backgrounds of the ZZZ process considered in this study.

SM process type	Selected backgrounds
P1: s-channel	$\rm H t\bar{t}, Z t\bar{t}, WW t\bar{t}, ZZH, ZHH, WWZ, HH, WWH, WWWW, WWZH, WWZZ$
P2.1: WW_VBS	$t\bar{t}$, WWH, ZHH, ZZH, ZZZ, WWZ, HH, ZZ, ZH
P2.2: ZZ_VBS	WW, ZH, ZZ, $t\bar{t}$, Z, H, WWZ
P2.3: WZ_VBS	WZ, WZH, WH, WWW, WZZ

signal yields, while suppressing backgrounds to a large extent. In this numerical analysis, we implemented the cut-based method. Some loose pre-selections were first applied to suppress events of no interest; subsequently, scans on each discriminating variable were performed to maximize signal sensitivity. In this numerical analysis, cut-based selections were optimized for each signal process.

IV. ZZZ DIRECT PRODUCTIONS AT A 1 TeV MUON COLLIDER

A. Pure-leptonic channel

To first suppress events of no interest, several pre-selections were applied: the event must include exactly four leptons with transverse momentum $p_{T,\ell} > 20\,\text{GeV}$, absolute pseudo-rapidity $|\eta_\ell| < 2.5$, and lepton pair geometrical separation of $\Delta R_{\ell\ell} > 0.4$, where $\Delta R = \sqrt{(\Delta\phi)^2 + (\Delta\eta)^2}$; $\Delta\phi$ and $\Delta\eta$ are the azimuthal angle separation and pseudorapidity separation of two particles, respectivly. The four leptons were classified and clustered into two reconstructed bosons (Z_1, Z_2), with their mass denoted as $M_{\ell\ell,1}, M_{\ell\ell,2}$, according to the following clustering algorithm:

• Construct all possible opposite sign lepton pair candidates: $(\ell_1\ell_2,\ \ell_3\ell_4)$ and $(\ell_1\ell_4, \ell_2\ell_3)$.

• Calculate the corresponding mass difference:

$$\Delta M_{4\ell} = |M_{\ell\ell,1} - M_Z| + |M_{\ell\ell,2} - M_Z|, \tag{4}$$

• Choose minimum $\Delta M_{4\ell}$ as the targeted lepton pairs and define $M_{\ell\ell,1} > M_{\ell\ell,2}$.

The selections for the further optimized signal over backgrounds are listed in Table 2, where variable $M_{4\ell}$ denotes the invariant mass of the four charged leptons decaying from two Z bosons; $M_{\ell\ell,1}$ and $M_{\ell\ell,2}$ are the invariant masses of two leptons decayed from reconstructed Z_1 and Z_2; $p_{T,4\ell}$ is the transverse momentum of four leptons decaying from two Z bosons; $p_{T,\ell\ell,1}$ and $p_{T,\ell\ell,2}$ are the transverse momentum of two leptons decayed from reconstructed Z_1 and Z_2; $\Delta R_{\ell\ell,1}$ and $\Delta R_{\ell\ell,2}$ are the geometrical separations of two leptons decayed from reconstructed Z_1 and Z_2; $|\eta_{\ell\ell,1}|$ and $|\eta_{\ell\ell,2}|$ are the absolute pseudorapidities of reconstructed Z_1 and Z_2; $p_{T,\ell}^{\text{leading}}$ denotes the highest p_T in the transverse momentum of the four charged leptons; $\not{E}_T$ is the missing transverse energy; and M_{recoil} is the recoil mass of four leptons, which can be calculated as

Table 2. Event selections for ZZZ in the pure-leptonic channel.

Variables	Limits for SM	Limits for aQGC
$M_{4\ell}$	[200 GeV, 900 GeV]	[150 GeV, 910 GeV]
$M_{\ell\ell,1}$	[80 GeV, 120 GeV]	[70 GeV, 130 GeV]
$M_{\ell\ell,2}$	[60 GeV, 100 GeV]	[40 GeV, 100 GeV]
$p_{T,4\ell}$	[30GeV, 480 GeV]	[30 GeV, 500 GeV]
$p_{T,\ell\ell,1}$	< 500 GeV	< 500 GeV
$p_{T,\ell\ell,2}$	< 460 GeV	< 500 GeV
$\Delta R_{\ell\ell,1}$	[0.4, 3.3]	[0.4, 3.1]
$\Delta R_{\ell\ell,2}$	[0.4, 3.3]	[0.4, 3.1]
$\lvert\eta_{\ell\ell,1}\rvert$	< 2.5	< 2.5
$\lvert\eta_{\ell\ell,2}\rvert$	< 2.5	< 2.5
$p_{T,\ell}^{\text{leading}}$	[20 GeV, 380 GeV]	[25 GeV, 460 GeV]
$\Delta M_{4\ell}$	< 20GeV	< 50 GeV
$\not{E}_T$	[50 GeV, 460 GeV]	[100 GeV, 480 GeV]
M_{recoil}	< 300 GeV	[35 GeV, 225 GeV]

$$M_{\text{recoil}} = \sqrt{(\sqrt{s} - E)^2 - P^2}. \tag{5}$$

Here, $\sqrt{s}$is the COM energy and E and P are the sum of the energy and momentum of the detectable daughter particles. In these selections, the SM and aQGC signals were optimized separately. For the SM signal, the efficiencies of the pure-leptonic and semi-leptonic channels were 0.75 and 0.34, respectively; for the aQGC signal, the efficiencies of the pure-leptonic and semi-leptonic channels were 0.82 and 0.40, respectively.

Figure 4 shows the typical distributions before all selections, including $M_{4\ell}$, $M_{\ell\ell,1}$, $\not{E}_T$, and M_{recoil}. We found that both $M_{\ell\ell,i}(i = 1,2)$ and M_{recoil} can distinguish signals and backgrounds well. For the SM signal, we obtained a significance [41] given by $\sqrt{2((s+b)\ln(1+s/b) - s)} = 0.9\sigma$, with S and B the denoting signal and background yields, respectively. The yield of the process was calculated by summing up the weights of the selected events, which were obtained from $\frac{\sigma \times \mathcal{L}}{N}$, where σ is the cross-section of the sample, $\mathcal{L}$ is the luminosity, and N is the total number of generated events. In these plots, we added curves for non-zero aQGCs, setting $f_{T,0}/\Lambda^4 = 100\ \text{TeV}^{-4}$ as a benchmark. In general, aQGCs lead to excess at high energy tails.

B. Semi-leptonic channel

A similar analysis was applied for the semi-leptonic channel, $ZZZ \to 4\ell + 2\text{jets}$. Figure 5 shows the distributions of $M_{4\ell}$, $M_{\ell\ell,1}$, the invariant mass of two jets decayed from the other Z boson, M_{jj}, and the transverse momentum of the jet pair, $p_{T,jj}$.

The selections of semi-leptonic channel are listed in

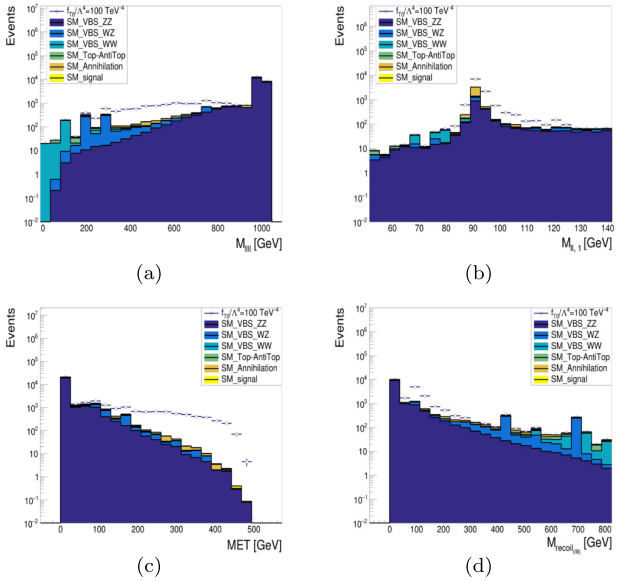

Fig. 4. (color online) Various distributions for the ZZZ direct productions in the pure-leptonic channel at a muon collider of $\sqrt{s} = 1\,\text{TeV}$ and $\mathcal{L} = 10\,\text{ab}^{-1}$: (a) invariant mass of four leptons, $M_{4\ell}$; (b) invariant mass of two leptons, $M_{\ell\ell,1}$; (c) missing transverse energy, $\not{E}_T$; and (d) recoil mass of four leptons, M_{recoil}.

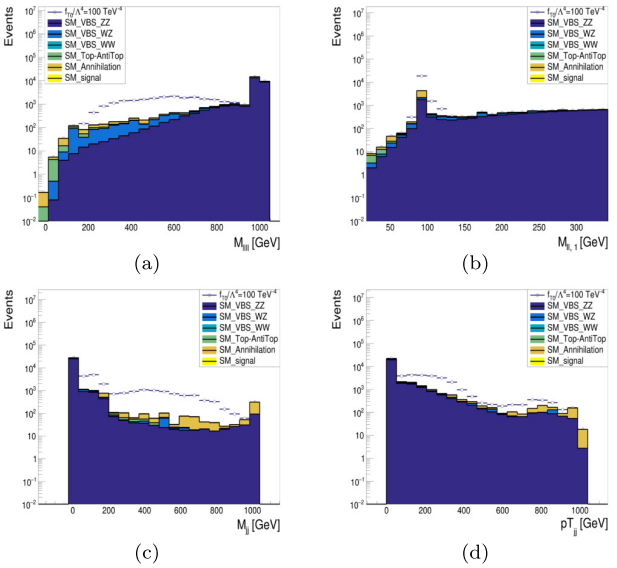

Fig. 5. (color online) Various distributions for the ZZZ direct productions in the semi-leptonic channel at a muon collider of $\sqrt{s} = 1\,\text{TeV}$ and $\mathcal{L} = 10\,\text{ab}^{-1}$: (a) invariant mass of four leptons, $M_{4\ell}$ distribution; (b) invariant mass of two leptons, $M_{\ell\ell,1}$; (c) invariant mass of two jets, M_{jj}; and (d) transverse momentum of two jets in final state, $p_{T,jj}$ distribution.

Table 3, where ΔR_{jj} is the geometrical separation of two jets; $|\eta_{jj}|$ is the absolute pseudorapidity of the Z boson reconstructed from two jets; and $p_{T,j}^{\text{leading}}$ denotes the highest value of p_T in the transverse momentum of two jets.

Table 3. Event selections for ZZZ in the semi-leptonic channel.

Variables	Limits for SM	Limits for aQGC
$M_{4\ell}$	[200 GeV, 840 GeV]	[150 GeV, 930 GeV]
$M_{\ell\ell,1}$	[80 GeV, 120 GeV]	[85 GeV, 130 GeV]
$M_{\ell\ell,2}$	[60 GeV, 100 GeV]	[65 GeV, 115 GeV]
M_{jj}	< 150 GeV	[30 GeV, 150 GeV]
$p_{T,4\ell}$	[30 GeV, 450 GeV]	[30 GeV, 480 GeV]
$p_{T,\ell\ell,1}$	< 500 GeV	< 480 GeV
$p_{T,\ell\ell,2}$	< 460 GeV	< 480 GeV
$p_{T,jj}$	< 420 GeV	< 500 GeV
$\Delta R_{\ell\ell,1}$	[0.4, 3.1]	[0.4, 3.3]
$\Delta R_{\ell\ell,2}$	[0.4, 3.1]	[0.4, 3.3]
ΔR_{jj}	[0.4, 4.0]	[0.4, 3.5]
$\lvert\eta_{\ell\ell,1}\rvert$	< 2.5	< 2.5
$\lvert\eta_{\ell\ell,2}\rvert$	< 2.5	< 2.5
$\lvert\eta_{jj}\rvert$	< 5.0	< 5.0
$p_{T,\ell}^{\text{leading}}$	[20 GeV, 400 GeV]	[20 GeV, 420 GeV]
$p_{T,j}^{\text{leading}}$	[30 GeV, 480 GeV]	[30 GeV, 510 GeV]
$\Delta M_{4\ell}$	< 20 GeV	< 30 GeV
$\not{E}_T$	< 100 GeV	< 150 GeV
M_{recoil}	< 300 GeV	[35 GeV, 225 GeV]

The selections improve the significance of both SM and aQGC signals. With $10\,\text{ab}^{-1}$ of integrated luminosity at $\sqrt{s} = 1\,\text{TeV}$, the expected yields of the SM signal and background after the selections are listed in Table 4; concerning the aQGC benchmark, with $f_{T,0}/\Lambda^4 = 100\ \text{TeV}^{-4}$, the expected yields of the aQGC signal and background after the selections are listed in Table 5.

After the selections, the significance for this semi-leptonic channel can reach 1.7σ for the SM signal process. We further combined the pure-leptonic and semi-leptonic channels, resulting in a higher significance of 1.9σ for the SM signal. We also searched for aQGCs, obtaining the constraint range of all coefficients $f_{S,M,T}$, listed in Table 10.

V. VBS ZZ PRODUCTIONS AT A 10 TeV MUON COLLIDER

For the VBS ZZprocess, we performed simulation studies similar to those for the ZZZ process. We considered both pure-leptonic ($\mu^+\mu^- \to \text{ZZ}\nu_\mu\bar{\nu}_\mu \to 4\ell + \nu_\mu\bar{\nu}_\mu$) and semi-leptonic ($\mu^+\mu^- \to \text{ZZ}\nu_\mu\bar{\nu}_\mu \to 2\ell 2j + \nu_\mu\bar{\nu}_\mu$) channels. The backgrounds were also divided into P1 (s-channel), P2.1 (WW_VBS), P2.2 (ZZ_VBS), and P2.3 (WZ_VBS). They are listed in Table 6.

Table 4. Expected yields of the SM signal and background after the selections in the ZZZ direct productions.

Channels ($\sqrt{s} = 1$ TeV)	Expected signal yield [events]	Expected background yield [events]
Pure-leptonic channel	5.18	31.72
Semi-leptonic channel	4.48	5.46

Table 5. Expected yields of the aQGC signal and background after the selections in the ZZZ direct productions.

Channels ($\sqrt{s} = 1$ TeV)	Expected signal yield [events]	Expected background yield [events]
Pure-leptonic channel	5514.90	56.80
Semi-leptonic channel	6271.79	9.16

Table 6. Summary of the backgrounds for the VBS ZZ process.

SM process type	Selected backgrounds
P1: s-channel	WW, ZZ, ZH, HH, ZHH, ZZZ, ZZH, WWH, WWZ, $t\bar{t}$, H$t\bar{t}$, Z$t\bar{t}$, WW$t\bar{t}$, WWWW, WWZH, WWHH
P2.1: WW_VBS	WW, ZH, HH, WWH, WWZ, ZZZ, ZZH, ZHH, $t\bar{t}$, Z, H
P2.2: ZZ_VBS	WW, ZH, ZZ, $t\bar{t}$, Z, WWH, WWZ, H, HH, ZZZ, ZZH, ZHH
P2.3: WZ_VBS	WZ, WZH, WH, WWW, WZZ

A. Pure-leptonic channel of VBS ZZ

We applied pre-selections on the channel of $\mu^+\mu^- \to ZZ\nu_\mu\bar{\nu}_\mu \to 4\ell + \nu_\mu\bar{\nu}_\mu$ at a muon collider with $\sqrt{s} = 10$ TeV and $\mathcal{L} = 10\,\text{ab}^{-1}$, as in theZZZ analysis. The selections of the pure-leptonic channel are listed in Table 7. The signal efficiency of the selections was 0.23.

Figure 6 shows the distribution of the invariant mass of four leptons, denoted as $M_{4\ell}$, the invariant mass of two leptons, denoted as $M_{\ell\ell,1}$, the transverse momentum of four leptons in final states, denoted as $p_{T,4\ell}$, and the transverse momentum of one lepton pair, denoted as $p_{T,\ell\ell,1}$. In these plots, we also added curves for non-zero aQGCs, setting $f_{T,0}/\Lambda^4 = 1\,\text{TeV}^{-4}$ as a benchmark.

Table 7. Event selections for VBS ZZ in the pure-leptonic channel.

Variables	Limits
$M_{4\ell}$	[1900 GeV, 8800 GeV]
$M_{\ell\ell,1}$	[70 GeV, 140 GeV]
$M_{\ell\ell,2}$	[70 GeV, 140 GeV]
$p_{T,4\ell}$	[200 GeV, 4000 GeV]
$p_{T,\ell\ell,1}$	[320 GeV, 2800 GeV]
$p_{T,\ell\ell,2}$	[280 GeV, 2600 GeV]
$\Delta R_{\ell\ell,1}$	[0.4, 1.7]
$\Delta R_{\ell\ell,2}$	[0.4, 1.7]
$\lvert\eta_{\ell\ell,1}\rvert$	< 2.5
$\lvert\eta_{\ell\ell,2}\rvert$	< 2.5
$p_{T,\ell}^{\text{leading}}$	[200 GeV, 3000 GeV]
$\Delta M_{4\ell}$	< 70 GeV
$\not{E}_T$	[30 GeV, 4000 GeV]
M_{recoli}	< 8000 GeV

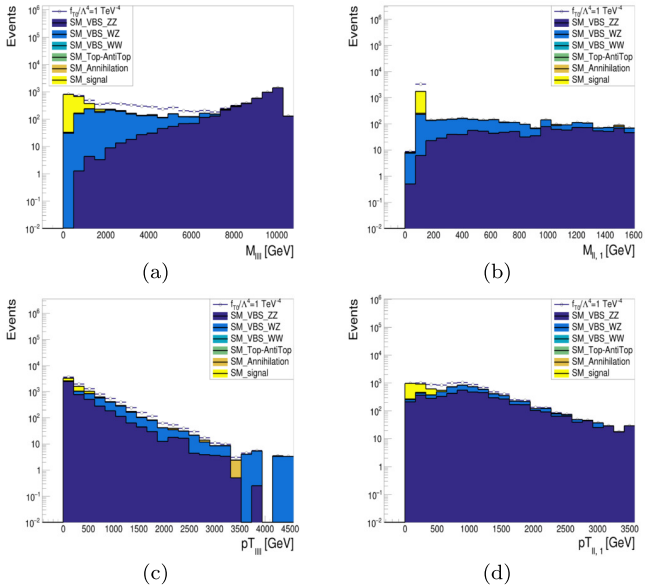

Fig. 6. (color online) Simulation results of VBS ZZ in the pure-leptonic channel for $\sqrt{s} = 10$ TeV, $\mathcal{L} = 10\,\text{ab}^{-1}$: (a) invariant mass of four leptons, $M_{4\ell}$ distribution; (b) invariant mass of two leptons, $M_{\ell\ell,1}$; (c) transverse momentum of four leptons, $p_{T,4\ell}$ distribution; and (d) transverse momentum of two leptons, $p_{TT,\ell\ell,1}$ distribution.

B. Semi-leptonic channels of VBS ZZ

The selections in the semi-leptonic channel are listed in Table 8, where $M_{2\ell 2j}$ is the invariant mass of two leptons and two jets decaying from two Z bosons; $\Delta M_{2\ell 2j}$

Table 8. Event selections for VBS ZZ in the semi-leptonic channel.

Variables	Limits
$M_{2\ell 2j}$	[2000 GeV, 8000 GeV]
$M_{\ell\ell}$	[40 GeV, 140 GeV]
M_{jj}	[30 GeV, 150 GeV]
$p_{T,2\ell 2j}$	[500 GeV, 8000 GeV]
$p_{T,\ell\ell}$	[200 GeV, 3000 GeV]
$p_{T,jj}$	[400 GeV, 4000 GeV]
$\Delta R_{\ell\ell}$	[0.4, 1.7]
ΔR_{jj}	> 0.4
$\lvert\eta_\ell\rvert$	< 2.5
$\lvert\eta_j\rvert$	< 5.0
$p_{T,\ell}^{\text{leading}}$	[200 GeV, 2500 GeV]
$p_{T,j}^{\text{leading}}$	[200 GeV, 3000 GeV]
$\Delta M_{2\ell 2j}$	< 200 GeV
$\not{E}_T$	[30 GeV, 3500 GeV]
M_{recoli}	[1000 GeV, 7000 GeV]

is the mass difference, defined as follows:

$$\Delta M_{2\ell 2j} = |M_{\ell\ell} - M_Z| + |M_{jj} - M_Z|, \tag{6}$$

The signal efficiency of the selections was 0.033.

Figure 7 shows distributions of the invariant mass of jet pair, denoted as M_{jj}, lepton pair mass, denoted as $M_{\ell\ell}$, together with the aQGC signal with coefficient $f_{T,0}/\Lambda^4 = 1\,\text{TeV}^{-4}$.

After applying the above selections, the significance of the aQGC signal was improved. With $10\,\text{ab}^{-1}$ of integrated luminosity at $\sqrt{s} = 10\,\text{TeV}$ and aQGC benchmark with $f_{T,0}/\Lambda^4 = 1\,\text{TeV}^{-4}$, the expected yields of the aQGC signal and background after the selections are listed in Table 9.

We also obtained the limits of all aQGC coefficients of the VBS ZZ process, which are listed in Table 11.

VI. RESULTS AND DISCUSSIONS

We studied the multi-Z productions of ZZZ at a muon collider with $\sqrt{s} = 1\,\text{TeV}$ and $\mathcal{L} = 10\,\text{ab}^{-1}$. Through detailed simulations and signal background analysis, we obtained a significance for the ZZZ direct production in the SM of 1.9σ after combining the results from the pure-leptonic and semi-leptonic channels. We also set the constraints of the aQGC coefficients [42] at 95% CL. High-energy muon colliders are ideal to research VBS processes, such as the VBS ZZ production process. We presented the distribution of various variables and summarized the constraints of aQGC coefficients. For the

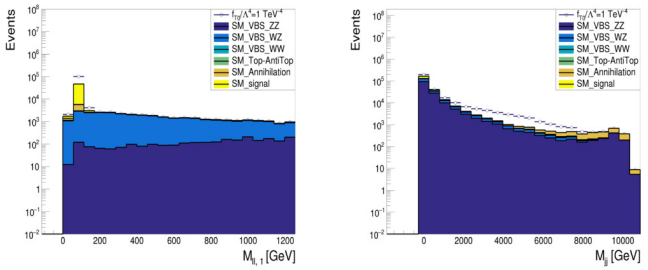

(a) (b)

Fig. 7. (color online) Simulation results of VBS ZZin the semi-leptonic channel for $\sqrt{s} = 10\,\text{TeV}, \mathcal{L} = 10\,\text{ab}^{-1}$: (a) invariant mass of two leptons, $M_{\ell\ell}$ distribution; and (b) invariant mass of two leptons, M_{jj}.

Table 9. Expected yields of the aQGC signal and background after the selections in the VBS ZZ productions.

Channels ($\sqrt{s} = 10\,\text{TeV}$)	Expected signal yield [events]	Expected background yield [events]
Pure-leptonic channel	686.97	0.48
Semi-leptonic channel	315.40	0.15

Table 10. Limits at the 95% CL on the aQGC coefficients for the ZZZ process.

Coefficient	Constraint /TeV^{-4}
$f_{S,0}/\Lambda^4$	[−211, 366]
$f_{S,1}/\Lambda^4$	[−207, 364]
$f_{S,2}/\Lambda^4$	[−213, 364]
$f_{M,0}/\Lambda^4$	[−13.2, 30.4]
$f_{M,1}/\Lambda^4$	[−36.7, 22.9]
$f_{M,2}/\Lambda^4$	[−11.8, 13.0]
$f_{M,3}/\Lambda^4$	[−23.1, 20.6]
$f_{M,4}/\Lambda^4$	[−26.2, 36.8]
$f_{M,5}/\Lambda^4$	[−22.5, 31.5]
$f_{M,7}/\Lambda^4$	[−43.3, 69.9]
$f_{T,0}/\Lambda^4$	[−4.63, 3.28]
$f_{T,1}/\Lambda^4$	[−4.51, 3.34]
$f_{T,2}/\Lambda^4$	[−9.38, 5.84]
$f_{T,3}/\Lambda^4$	[−9.22, 6.00]
$f_{T,4}/\Lambda^4$	[−14.8, 11.5]
$f_{T,5}/\Lambda^4$	[−7.01, 5.95]
$f_{T,6}/\Lambda^4$	[−7.00, 6.06]
$f_{T,7}/\Lambda^4$	[−14.9, 11.6]
$f_{T,8}/\Lambda^4$	[−5.25, 5.04]
$f_{T,9}/\Lambda^4$	[−10.4, 9.66]

ZZZ process, the constraints of coefficients at 95% CL are listed in Table 10, whereas for the VBS ZZ produc-

Table 11. Limits at the 95% CL on the aQGC coefficients for the VBS ZZ process.

Coefficient	Constraint /TeV^{-4}
$f_{S,0}/\Lambda^4$	$[-14,13]$
$f_{S,1}/\Lambda^4$	$[-5.8,6.7]$
$f_{S,2}/\Lambda^4$	$[-15,16]$
$f_{M,0}/\Lambda^4$	$[-1.2,1.1]$
$f_{M,1}/\Lambda^4$	$[-3.9,3.7]$
$f_{M,2}/\Lambda^4$	$[-8.0,8.2]$
$f_{M,3}/\Lambda^4$	$[-3.9,3.8]$
$f_{M,4}/\Lambda^4$	$[-3.3,3.2]$
$f_{M,5}/\Lambda^4$	$[-2.9,3.0]$
$f_{M,7}/\Lambda^4$	$[-8.3,8.1]$
$f_{T,0}/\Lambda^4$	$[-0.11,0.082]$
$f_{T,1}/\Lambda^4$	$[-0.14,0.14]$
$f_{T,2}/\Lambda^4$	$[-0.27,0.21]$
$f_{T,3}/\Lambda^4$	$[-0.27,0.22]$
$f_{T,4}/\Lambda^4$	$[-1.1,0.67]$
$f_{T,5}/\Lambda^4$	$[-0.32,0.25]$
$f_{T,6}/\Lambda^4$	$[-0.47,0.42]$
$f_{T,7}/\Lambda^4$	$[-0.89,0.60]$
$f_{T,8}/\Lambda^4$	$[-0.47,0.48]$
$f_{T,9}/\Lambda^4$	$[-1.1,1.0]$

tion process, the constraints of the aQGC coefficients at 95% CL are listed in Table 11; the unit is TeV^{-4}.

In the ZZZ direct productions, some operators degenerate, such as f_{S0}, f_{S1}, and f_{S2}; f_{T0} and f_{T1}; and f_{T5} and f_{T6}. However, we kept all the constraints in Table 10 for the completeness of the set of operator coefficients.

In comparison with existing VBS ZZ aQGC constraints from the CMS experiment in LHC, which are based on a data sample of proton-proton collisions at COM = 13 TeV with an integrated luminosity of $\mathcal{L}$ = 137 fb^{-1} : $f_{T,0}/\Lambda^4 : [-0.24,0.22]$, $f_{T,1}/\Lambda^4 : [-0.31,0.31]$, $f_{T,2}/\Lambda^4 : [-0.63,0.59]$[43], our results establish stronger limits: $f_{T,0}/\Lambda^4 : [-0.11,0.082]$, $f_{T,1}/\Lambda^4 : [-0.14,0.11]$, $f_{T,2}/\Lambda^4 : [-0.27,0.21]$.

VII. CONCLUSIONS AND OUTLOOK

In this study, we investigated ZZZ productions at a muon collider with $\sqrt{s} = 1\,\text{TeV}, \mathcal{L} = 10\,\text{ab}^{-1}$ and VBS ZZ productions at $\sqrt{s} = 10\,\text{TeV}, \mathcal{L} = 10\,\text{ab}^{-1}$, together with their sensitivities on aQGC coefficients. For these two processes, we focused on pure-leptonic and semi-leptonic channels to find the kinematic features that help to increase the detection potential, such as the distribution of $M_{\ell\ell}$ in the pure-leptonic channel and M_{jj} in the semi-leptonic channel. We studied the constraints of all aQGC coefficients at 95% CL. For the ZZZ process, we supplemented the existing tri-boson aQGC results, and for some coefficients such as $f_{T,0}, f_{T,1}, f_{T,2}$ in the VBS ZZ process, our results establish stronger limits than those from previous results. The results demonstrate a great potential to probe the anomalous interactions of gauge bosons at muon colliders owing to their higher effective collision energy, cleaner final states, and higher probability to emit EW radiation than LHC.

References

[1] D. R. Green, P. Meade, and M. A. Pleier, Rev. Mod. Phys. **89**(3), 035008 (2017), arXiv: 1610.07572 [hep-ex]

[2] G. Aad *et al.* (ATLAS Collaboration), Phys. Lett. B **716**, 1 (2012)

[3] S. Chatrchyan *et al.* (CMS Collaboration), Phys. Lett. B **716**, 30 (2012), arXiv: 1207.7235 [hep-ex]

[4] T. Roser, R. Brinkmann, S. Cousineau *et al.*, JINST **18**(05), P05018 (2023), arXiv: 2208.06030 [physics.acc-ph]

[5] K. Long, D. Lucchesi, M. Palmer *et al.*, Nature Phys. **17**(3), 289 (2021), arXiv: 2007.15684 [physics.acc-ph]

[6] J. de Blas *et al.* (International Muon Collider

Collaboration), arXiv: 2203.07261 [hep-ph]
[7] C. Accettura, D. Adams, R. Agarwal *et al*., Eur. Phys. J. C **83**, 864(2023), [Erratum: Eur. Phys. J. C 84, 36 (2024)], arXiv: 2303.08533 [physics.acc-ph]
[8] H. Amarkhail, S. C. Inan, and A. V. Kisselev, arXiv: 2306.03653 [hep-ph]
[9] J. C. Yang, X. Y. Han, Z. B. Qin *et al*., JHEP **09**, 074 (2022), arXiv: 2204.10034 [hep-ph]
[10] J. C. Yang, Z. B. Qing, X. Y. Han *et al*., JHEP **22**, 053 (2020), arXiv: 2204.08195 [hep-ph]
[11] Y. F. Dong, Y. C. Mao, i. C. Yang *et al*., Eur. Phys. J. C **83**(7), 555 (2023), arXiv: 2304.01505 [hep-ph]
[12] S. Zhang, J. C. Yang, and Y. C. Guo, Eur. Phys. J. C **84**(2), 142 (2024), arXiv: 2302.01274 [hep-ph]
[13] S. Jahedi and J. Lahiri, JHEP **04**, 085 (2023), arXiv: 2212.05121 [hep-ph]
[14] S. Jahedi, JHEP **12**, 031 (2023), arXiv: 2305.11266 [hep-ph]
[15] P. Langacker, Adv. Ser. Direct. High Energy Phys. **14**, 883 (1995), arXiv: hep-ph/9412361 [hep-ph]
[16] O. J. P. Eboli, M. C. Gonzalez-Garcia, and S. M. Lietti, Phys. Rev. D **69**, 095005 (2004), arXiv: hep-ph/0310141 [hep-ph]
[17] C. Degrande, N. Greiner, W. Kilian *et al*., Annals Phys. **335**, 21 (2013), arXiv: 1205.4231 [hep-ph]
[18] C. Degrande, JHEP **02**, 101 (2014), arXiv: 1308.6323 [hep-ph]
[19] A. M. Sirunyan *et al*. (CMS Collaboration), Phys. Rev. Lett. **125**, 151802 (2020), arXiv: 2006.11191 [hep-ex]
[20] J. M. Kunkle, arXiv: 1511.00143 [hep-ex]
[21] G. Belanger and F. Boudjema, Phys. Lett. B **288**, 201 (1992)
[22] C. Arzt, M. B. Einhorn, and J. Wudka, Nucl. Phys. B **433**, 41 (1995), arXiv: hep-ph/9405214 [hep-ph]
[23] A. S. Belyaev, O. J. P. Eboli, M. C. Gonzalez-Garcia *et al*., Phys. Rev. D **59**, 015022 (1999), arXiv: hep-ph/9805229 [hep-ph]
[24] O. J. P. Eboli, M. C. Gonzalez-Garcia, S. M. Lietti *et al*., Phys. Rev. D **63**, 075008 (2001), arXiv: hep-ph/0009262 [hep-ph]
[25] O. J. P. Eboli, M. C. Gonzalez-Garcia, and J. K. Mizukoshi, Phys. Rev. D **74**, 073005 (2006), arXiv: hep-ph/0606118 [hep-ph]
[26] G. Belanger, F. Boudjema, Y. Kurihara *et al*., Eur. Phys. J. C **13**, 283 (2000), arXiv: hep-ph/9908254 [hep-ph]
[27] O. J. P. Éboli and M. C. Gonzalez-Garcia, Phys. Rev. D **93**(9), 093013 (2016), arXiv: 1604.03555 [hep-ph]
[28] C. Degrande, O. Eboli, B. Feigl *et al.*, arXiv: 1309.7890[hep-ph]
[29] M. Baak, A. Blondel, A. Bodek *et al.*, arXiv: 1310.6708 [hep-ph]
[30] E. d. Almeida, O. J. P. Éboli, and M. C. Gonzalez-Garcia, Phys. Rev. D **101**(11), 113003 (2020), arXiv: 2004.05174 [hep-ph]
[31] R. Frederix and S. Frixione, JHEP **12**, 061 (2012), arXiv: 1209.6215 [hep-ph]
[32] J. Alwall, R. Frederix, S. Frixione *et al*., JHEP **07**, 079 (2014), arXiv: 1405.0301 [hep-ph]
[33] C. Bierlich, S. Chakraborty, N. Desai *et al*., SciPost Phys. Codeb. **2022**, 8 (2022), arXiv: 2203.11601 [hep-ph]
[34] A. Alloul, N. D. Christensen, C. Degrande *et al*., Comput. Phys. Commun. **185**, 2250 (2014)
[35] C. Degrande, C. Duhr, B. Fuks *et al*., Comput. Phys. Commun. **183**, 1201 (2012)
[36] J. de Favereau *et al*. (DELPHES 3 Collaboration), JHEP **02**, 057 (2014)
[37] https://github.com/delphes/delphes/blob/master/cards/delphes_card_MuonColliderDet.tcl retrieved 3rd April 2024
[38] M. Cacciari, G. P. Salam, and G. Soyez, Eur. Phys. J. C **72**, 1896 (2012), arXiv: 1111.6097 [hep-ph]
[39] A. Costantini, F. De Lillo, F. Maltoni *et al*., JHEP **09**, 080 (2020), arXiv: 2005.10289 [hep-ph]
[40] T. Yang, S. Qian, Z. Guan *et al*., Phys. Rev. D **104**(9), 093003 (2021), arXiv: 2107.13581 [hep-ph]
[41] G. Cowan, K. Cranmer, E. Gross *et al*., Eur. Phys. J. C **71**, 1554 (2011), [Erratum: Eur. Phys. J. C 73, 2501 (2013)]
[42] https://feynrules.irmp.ucl.ac.be/attachment/wiki/AnomalousGaugeCoupling/quarticCKM21v2.tgz retrieved 3rd April 2024
[43] A. M. Sirunyan *et al*. (CMS Collaboration), Phys. Lett. B **812**, 135992 (2021), arXiv: 2008.07013 [hep-ex]